

Tuning superconductivity in vanadium nitride films by adjusting strain

Yuting Zou,^{1,2} Qiao Jin,^{1,2} Yuxin Wang,^{1,2} Kun Jiang,^{1,2,3} Shanmin Wang,⁴ Yangmu Li,^{1,2}
Er-Jia Guo,^{1,2,3} and Zhi Gang Cheng^{1,2,3,*}

¹Beijing National Laboratory for Condensed Matter Physics, Institute of Physics, Chinese Academy of Sciences, Beijing 100190, China

²School of Physical Sciences, University of Chinese Academy of Sciences, Beijing 100049, China

³Songshan Lake Materials Laboratory, Dongguan, Guangdong 523808, China

⁴Department of Physics, Southern University of Science and Technology, Shenzhen, Guangdong 518055, China



(Received 29 November 2021; revised 18 April 2022; accepted 15 June 2022; published 29 June 2022)

Transition-metal nitrides (TMNs) are enriched with various exotic phenomena such as superconductivity and quantum magnetism. Vanadium nitride (VN) is a typical superconducting TMN, with its superconductivity sensitively associated with various physical and chemical factors including nitrogen vacancies and lattice constants. Strain tuning is a convenient and effective method to manipulate the superconducting behavior of VN in the thin-film form, providing an additional tuning knob for potential applications in quantum computing and passive microwave devices. Here, we demonstrate the effect of strain tuning on VN films both statically and dynamically. By depositing on various substrates, the static strain states of VN films can be controlled from -4.04% (compressive) to $+2.0\%$ (tensile), making the superconducting transition temperature (T_c) tunable by approximately $\pm 10\%$. Applying *in situ* dynamic compressive strain via a piezoelectric substrate, we are able to achieve control of T_c by a step as fine as 10 mK. Furthermore, our first-principles calculations point out that the strain-tuning effect of T_c originates from a change in the density of states for vanadium's d orbitals.

DOI: [10.1103/PhysRevB.105.224516](https://doi.org/10.1103/PhysRevB.105.224516)

I. INTRODUCTION

Transition-metal nitrides (TMNs) are a large group of materials with importance in not only fundamental research but also in practical applications. Members of this family exhibit exotic physical properties such as superconductivity [1–3] and quantum magnetism [4–7], as well as excellent mechanical properties, thermal stability, and chemical resistance [8,9]. Besides the advantages in physical and mechanical properties, many TMNs can be epitaxially grown on various substrates in the form of thin films, which provides great potential in technical and industrial applications, including data storage, complementary metal-oxide semiconductor technology (as barrier layers), and electrodes for supercapacitors [10–13].

Superconductivity has been observed for several members of the TMN family with NaCl-cubic ($Fm\bar{3}m$) structure, including titanium nitride (TiN), zirconium nitride, vanadium nitride (VN), and niobium nitride (NbN). NbN's superconducting transition takes place at $T_c = 17.3$ K, higher than the others and well above liquid helium temperature [2]. Its upper critical magnetic field (H_{c2}) reaches 16 T [14], making it a reliable superconducting material for various low-temperature applications. Superconductivity of its derivative with Ti incorporated—niobium titanium nitride (NbTiN)—is further improved, enabling the fabrication of high-field superconducting magnets [15]. A recent experiment demonstrates the existence of Cooper pairs at temperatures above T_c by integrating shot-noise measurements in scanning tunneling microscopy [16]. On the other hand, T_c of VN is only 8.9 K

[17] while the prediction based on Bardeen-Cooper-Schrieffer theory is 32 K [2,3] given its strong electron-phonon coupling [2,17,18]. The tremendous suppression of T_c is claimed to be associated with strong spin fluctuations inferred by its enhanced magnetic susceptibility [19,20].

The emergence of superconductivity in VN depends on various factors. Previous reports demonstrate that VN with a stoichiometric chemical composition exhibits higher T_c , while it decreases with an increasing amount of nitrogen vacancies [3,19,21] that simultaneously leads to chemical environment change and lattice shrinking. Interestingly, a recent experiment demonstrates that T_c can be enhanced by applying hydrostatic pressure on bulk VN up to 8 GPa [18], suggesting that nitrogen orbitals participate in the electronic conduction and play an important role in superconductivity.

Superconducting thin films are of greater importance for practical applications such as superconducting quantum computations, superconducting quantum interference devices, and single-photon detectors [22]. The capability of tuning superconductivity can be a powerful tool in manipulating and controlling superconducting devices. For example, it is possible to intake or expel quantum flux from Josephson junctions by switching between superconducting and normal states. In comparison with bulk materials, thin films have much more flexibility to control a variety of parameters, such as charge carrier density, conformality to curve surfaces, etc. Among these, strain is an important parameter for tuning, and it can be conveniently realized by making use of the lattice misfit between films and substrates. In addition, dynamic and reversible strain tuning can be achieved if the films are deposited on piezoelectric substrates, whose lattice constant can be adjusted by electric fields.

*zgcheng@iphy.ac.cn

Here we report our study on the effect of strain tuning on the superconductivity in VN thin films. By depositing VN thin films on various substrates with different lattice constants and on piezoelectric substrates, the strain of VN films can be controlled both statically and dynamically. We found that T_c of VN films is enhanced by in-plane tensile strain and suppressed by compressive strain. First-principles calculations show that the majority of itinerant electrons in VN are from vanadium's $3d$ orbitals. Application of tensile strain increases the density of states (DOS) of the d_{xy} and $d_{x^2-y^2}$ orbitals, both lying in-plane and relevant to electrical transport and superconductivity. From the practical application viewpoint, *in situ* dynamical strain tuning can enable possible applications for quantum computations and passive microwave devices based on VN films. A similar device structure can also be employed for other superconducting TMNs.

II. EXPERIMENTAL METHODS AND RESULTS

VN films were grown on (001)-oriented MgO, KTaO₃ (KTO), and (110)-oriented GdScO₃ (GSO) substrates simultaneously by active nitrogen-assisted pulsed laser deposition. A stoichiometric ceramic VN was used as a target. To obtain highly crystalline VN thin films, the growth conditions were optimized by systematically varying the growth temperature, laser fluence, and film-target distance. The best quality VN films were fabricated with the substrate-target distance of 7 cm, the substrate temperature of 700 °C, laser fluence of ~ 1.3 J/cm², and low base pressure of 1×10^{-8} Torr. Film thickness was controlled to be 50 unit cells (u.c.) (approximately 20 nm) by counting the number of laser pulses. Samples on MgO, GSO, and KTO were grown simultaneously in order to guarantee the same chemical composition. The films were cooled down at a rate of -5 °C/min in vacuum after completion of the synthesis. Lattice constants of MgO, KTO, and GSO (taken from its pseudocubic unit cell) are 4.216, 3.989, and 3.965 Å, respectively. Based on the intrinsic lattice constant of 4.132 Å for bulk VN, the in-plane misfit strains are +2.03%, -3.46%, and -4.04% for films deposited on these three substrates. Here the “+” sign indicates tensile strains, and the “-” sign indicates compressive strains.

Electric transport measurements were performed using Van der Pauw method with cold-welded contacts of indium. A standard lock-in technique was used with frequency of 17 Hz and current of 1 μ A. Measurements were performed in a physical properties measurement system (Quantum Design) between 300 and 2 K and in a dilution refrigerator (Triton500; Oxford Instruments) between 20 and 0.02 K.

A. Static strain tuning

The temperature dependence of resistivities for the VN thin films is plotted in Fig. 1(a). All films exhibit metallic behavior below 300 K and superconducting transitions at low temperatures (T_c). A mild linear temperature dependence exists roughly between 300 and 150 K, which gradually transits to a steeper linear region between 100 and 50 K, and saturates below 50 K until T_c is reached. The slope change at 100–150 K is reported to be associated with a structural

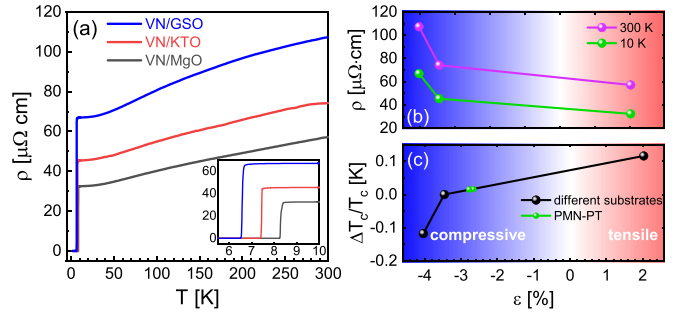


FIG. 1. (a) Temperature dependence of resistivity for VN thin films grown on various substrates. Inset: Zoom-in view of the superconducting transitions. (b) Strain dependence of resistivity (at 300 and 10 K) for VN films. (c) Relative change of T_c for VN films (black), compared to that of VN on KTO (7.40 K, $\Delta T_c = T_c - 7.40$ K). Normalized PMN-PT data (green) indicate the same quantity for VN deposited on the piezoelectric substrate, which will be discussed later in the text.

transition from cubic to tetragonal unit cell [23]. In our thin films, the transitions take place at lower temperatures than previously reported results possibly due to the strain effect from substrates as our films are much thinner. With the substrate lattice constant decreasing from MgO to GSO, the resistivity of deposited VN films increases.

Superconducting transitions of the three samples are shown in the inset of Fig. 1(a). $T_c = 8.26$, 7.40, and 6.53 K for thin films deposited on the substrates of MgO, KTO, and GSO, respectively. Remarkably, T_c exhibits a monotonic dependence on the strain, and it can be enhanced by tensile strain and reduced by compressive strain by approximately 10% of its value. This strain dependence of T_c seems closely related to that of the resistivity, as summarized in Figs. 1(b) and 1(c). To rule out large structural and chemical composition differences in the three samples, we carried out x-ray scattering and energy dispersive x-ray spectroscopy (EDX) measurements, which found good crystallinity and less than 2.3% variation of V and N across the three samples (see Supplemental Material [24]). This variation is too small to account for the change in T_c and resistivity. Alternatively, T_c and resistivity can also be impacted by disorders such as excess nitrogen or vacancies, even when the chemical change is small. Typically, such disorders would result in a broadening of superconducting transition, and the transition should become much wider in temperature for samples with higher resistivity. For all of our VN films, the width of superconducting transition in temperature is about 200 mK; much smaller than the value of T_c . These results indicate that neither chemical composition nor disorder is the main factor in controlling T_c . Instead, T_c has a systematic dependence on the in-plane strain. We note that although strain likely provides the largest tuning of T_c and resistivity, other factors can have a secondary effect. For VN film on GSO, for example, whose T_c has the lowest value and deviates from the strain dependence of other films, our x-ray measurements find a decrease in the VN Bragg peak intensity, suggesting a structural instability due to large strain (see Supplemental Material [24]).

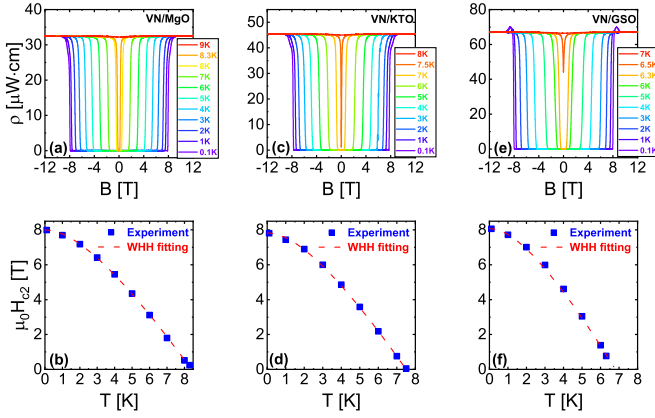


FIG. 2. (a),(c),(e) Magnetoresistance measurements of VN films on MgO, KTO, and GSO substrates, respectively. (b),(d),(f) Temperature dependence of the upper critical fields $\mu_0 H_{c2}$ for each sample. Red dashed lines represent fitting curves based on the WHH model.

The upper critical magnetic fields of all three samples were determined by magnetoresistance measurements. The magnetic field perpendicular to the film was swept at a rate of 0.1 T/min from -12 to $+12$ T with temperature fixed at values from 0.1 K up to T_c . $\mu_0 H_{c2}$ was determined at fields when resistivity decreases to its half normal-state value. Notably, although the variation of T_c is significant, critical fields for all three samples approach 8 T as the temperature is extrapolated to zero. We found that $\mu_0 H_{c2}$ does not exceed the Pauli limit ($B_p[T] = 1.84T_c[K] \geq 12$ T) [25], suggesting a dominating orbital effect. The convergence of critical field implies that the samples are within the dirty limit [26], as confirmed by the estimated superconducting coherence length ξ_0 around 300 nm, which is much larger than the mean free path (see Supplemental Material [24]). As shown in Fig. 2, the temperature dependence of the critical field can be well fitted by a single-band Werthamer-Helfand-Hohenberg (WHH) [27,28] equation:

$$\ln t + \psi\left(\frac{1}{2} + h\right) - \psi\left(\frac{1}{2}\right) = 0, \quad (1)$$

where $t = T/T_c$ is reduced temperature, $h = \frac{\mu_0 H_{c2} \hbar D}{2\phi_0 k_B T}$, D the diffusion coefficient, ϕ_0 the flux quantum, and ψ the digamma function. Here the spin-orbital coupling is assumed to be negligible considering both vanadium and nitrogen are relatively light elements. As a fitting parameter, diffusion coefficient D was determined to be 0.798, 0.728, and 0.640 cm^2/s for the samples on MgO, KTO, and GSO substrates, respectively. This is in qualitative agreement with the strain dependence of resistivity and T_c . Hall measurements were also performed at 10 K at which all films are in normal state. We found that the charge carriers are N-type for all samples, but the compressive strain clearly suppresses the carrier density. Being a maximum of $1.1 \times 10^{23} \text{ cm}^{-2}$ with MgO substrate with tensile strain, it drops by at least 20% when the misfit strain changes to be compressive. We summarize carrier densities, carrier mobilities, and related parameters in Table I.

TABLE I. Summary of parameters for VN thin films grown on substrates of MgO, KTO, and GSO, including lattice constant (a), in-plane strain (ϵ), superconducting transition temperature (T_c), resistivity (ρ), carrier density (n), carrier mobility (μ), and diffusion coefficient (D). Resistivity, carrier density, and mobilities are extracted by measurements at 10 K. Estimated errors are listed in parentheses.

	VN/MgO	VN/KTO	VN/GSO
a (Å)	4.216	3.989	3.965
ϵ (%)	+2.03	−3.46	−4.04
T_c (K)	8.261(4)	7.402(2)	6.530(2)
ρ ($\mu\Omega \text{ cm}$)	32.45(2)	45.40(1)	66.94(2)
n (10^{22} cm^{-3})	10.90(4)	10.00(2)	8.92(3)
μ ($\text{cm}^2/\text{V s}$)	1.76(3)	1.38(1)	1.05(1)
D (cm^2/s)	0.798	0.728	0.640

B. Dynamic strain tuning

In order to demonstrate dynamic and *in situ* strain tuning on superconductivity, we prepared another VN thin-film sample on a substrate of (001)-oriented $(1-x)\text{Pb}(\text{Mg}_{1/3}\text{Nb}_{2/3})\text{O}_{3-x}\text{PbTiO}_3$ (PMN-PT). The size of the PMN-PT substrate is $5 \times 5 \text{ mm}^2$, and the thickness of the sample is 50 u.c., the same as other samples in the present study. The back surface of the PMN-PT substrate was coated with a sputtered Pt film with a thickness of ~ 100 nm, and was attached to a copper plate with silver paint, making the copper plate as the electrode for tuning strain [see Fig. 3(a)]. PMN-PT is a perovskite-type ferroelectric single crystal with large piezoelectric coefficients. The lattice is composed of MO_6 octahedrons ($M = \text{Mg}, \text{Nb}, \text{Ti}$) in the form of a cubic lattice with shared oxygen corners and Pb atoms filled between. The unstrained in-plane lattice constant is 4.022 Å, exerting a compressive strain of -2.66% for the VN film. By applying a voltage across the substrate surface, the octahedrons will be stretched along applied electric field due to the separation of positive and negative charge centers. The polarization in either direction reduces the in-plane lattice constant from 4.022 to 4.017 Å, thus boosting the compressive strain on VN film from -2.66% to -2.78% .

The VN film on PMN-PT was firstly cooled down for measurements with the substrate unpolarized. To polarize the substrate, the sample was warmed up to room temperature and a voltage was ramped on the copper plate with the sample

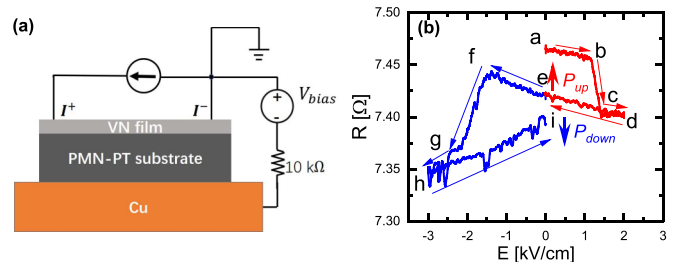


FIG. 3. (a) Experiment configuration of tuning polarization of PMN-PT substrate. (b) Process of tuning polarization while monitoring resistance of VN film at room temperature.

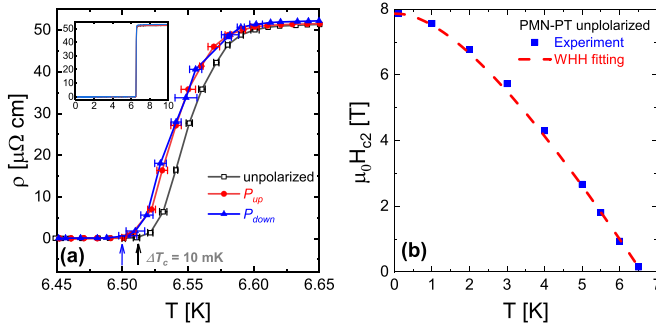


FIG. 4. (a) Temperature dependence of resistivity for the VN sample deposited on the PMN-PT substrate in unpolarized, P_{up} , and P_{down} states. The main panel exhibits the zoom-in view near the superconducting transition temperature, while the inset displays resistivity below 10 K. T_c is defined at which resistivity drops to zero, labeled by black (unpolarized) and blue (polarized) arrows. (b) Representative temperature dependence of the upper critical field for VN film on unpolarized PMN-PT substrate with a fit by the single-band WHH model. The data for VN film on polarized substrate are similar to the unpolarized case.

grounded. Polarization at room temperature is much easier than at low temperature since the coercive field is smaller. The coercive field at 4 K turns out to be beyond the threshold to damage the substrate. A positive (negative) V_{bias} generates an upwards (downwards) polarization. Electrical resistance of the VN sample was monitored simultaneously during the polarization process. As shown in Fig. 4(b), when first initializing the polarization, electrical resistance exhibits a mild decrease from “a” to “b”. This initialization process changes the lattice parameter of PMN-PT for the first time since the synthesis of VN film and allows a formation of polarization domains in the substrate. Following the initialization process, a sudden drop of resistivity is observed between “b” and “c”, which corresponds to a flip of PMN-PT polarization domains that are bounded by VN growth. Further increase of V_{bias} up to “d” leads to another mild decrease with the same rate as the “a-b” section when polarization domains are relatively stable, and V_{bias} is returned to zero (“e”) after reaching “d”, where the resistance is partially recovered. Only strain after the flip of polarization domains remains when V_{bias} reduces to zero. The mismatch of the resistance with zero V_{bias} at “a” and “e” is due to the initialization of polarization domains. The sample was cooled down for electrical transport measurements, and then warmed up to room temperature again for polarization in another direction (“e” to “i”). The film resistance exhibits similar behavior as the previous process, suggesting that polarization is successfully flipped. The coercive electric field for the PMN-PT substrate is around 1.5 kV/cm; smaller than reported by other studies [29–31]. The final resistance of the reversed ramping loop (at “i”) is smaller than that of the previous value (at “e”). Such a difference mostly stems from the large unexpected jumps in resistance when the bias field was swept beyond -2.4 kV/cm. The jumps may originate from the appearance of extra defects in PMN-PT substrates under the large bias field, which consequently create random defects or strain gradient in the VN film.

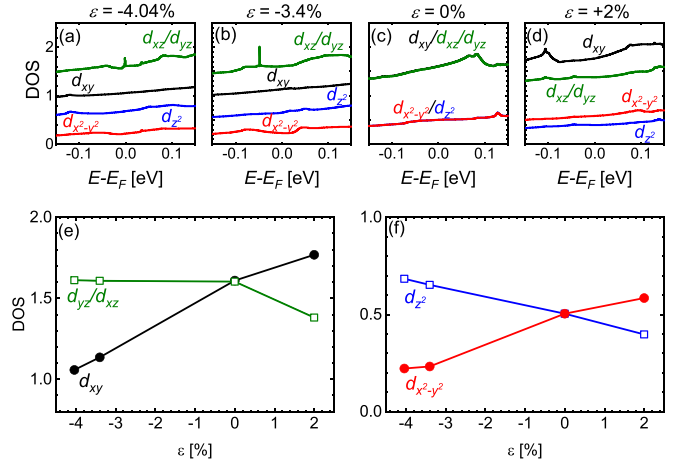


FIG. 5. (a)–(d) Calculations of density of state (DOS) for VN film at strains of -4.04% , -3.4% , 0% , and $+2.0\%$. (e), (f) Strain dependence of density of state at various d orbitals for vanadium.

Figure 4(a) exhibits the superconducting transitions of the VN film with the substrate at both unpolarized and polarized states. At the unpolarized state, superconducting transition takes place at $T_c = 6.51$ K, and polarization reduces it to 6.50 K. This is in qualitative agreement with the trend of strain tuning demonstrated by the VN on other different substrates. Note that for VN on PMN-PT, T_c is lower than that of the VN on KTO although its compressive strain is smaller. The lowering of T_c can be attributed to off-stoichiometry (7.4% less N), as measured by EDX and reported in previous studies [3,19,21,24]. For direct comparison, in Fig. 1(c), we normalize results for the PMN-PT substrate to that of the other VN films. On the other hand, its upper critical field in the zero-temperature limit still reaches about 8 T, suggesting this sample is still in the dirty limit [24], similar to other VN films. $\mu_0 H_{c2}$ vs T curves for polarized and unpolarized states almost collapse, so only the unpolarized state data are plotted in Fig. 5(b). These data are again well fitted by the single-band WHH model, and the extracted parameters at 10 K including diffusion coefficients, carrier densities, and mobilities are listed in Table II. The carrier density and mobility are slightly reduced by the polarization, consistent with a similar strain-tuning trend for the other three samples.

TABLE II. Summary of parameters and experimental results for the VN film on PMN-PT substrate before and after polarization. The resistivity, carrier density, and mobility are extracted by measurements at 10 K. Estimated errors are listed in parentheses.

	Unpolarized	P_{up}	P_{down}
a (Å)	4.022	4.017	4.017
ϵ (%)	-2.66	-2.78	-2.78
T_c (K)	6.510(2)	6.501(4)	6.501(3)
ρ ($\mu\Omega$ cm)	52.24(2)	52.33(4)	53.02(2)
n (10^{22} cm $^{-3}$)	9.60(3)	9.59(6)	9.58(4)
μ (cm 2 /V s)	1.24(4)	1.23(7)	1.23(5)
D (cm 2 /s)	0.637	0.627	0.625

C. Density-function theory calculations

We performed density-function theory (DFT) calculations to explore the mechanism of strain tuning on superconductivity. Because vanadium d orbitals contribute to the majority of itinerant electrons, the calculations focus on the evolution of the orbitals under strain. Crystal field splits d orbitals into t_{2g} and e_g bands, where the t_{2g} band is composed of d_{xy} , d_{yz} , and d_{xz} orbitals, and the e_g band is composed of $d_{x^2-y^2}$ and d_{z^2} orbitals. For an octahedral coordinate, the e_g band has higher energy than the t_{2g} band, with the energy split scaling with r^{-5} where r is the neighboring atom separation. As shown in Fig. 5(c), the DOS of the orbitals in the e_g band is lower than that in t_{2g} band for unstrained lattice. The degeneracy of each band is lifted when in-plane strain is induced. If considering disorders that can scatter the itinerant electrons, the main hopping path for itinerant electrons is between the vanadium d_{xy} and $d_{x^2-y^2}$ orbitals and the nitrogen p_x and p_y orbitals [3,19,21]. A compressive strain lifts the d_{xy} and $d_{x^2-y^2}$ orbitals to higher energies relative to the other orbitals, effectively reducing their DOS [see Figs. 5(a) and 5(b)]. The reduction of the population for these two orbitals, whose main distributions are in-plane, can lead to decreases in conductivity and T_c for VN films. Oppositely, a tensile strain lowers their energies and increases their populations [see Fig. 5(d)], leading to increases in conductivity and T_c .

III. SUMMARY

In summary, we have demonstrated the effects of strain tuning on the superconductivity of VN thin films. The in-

plane strain was statically tuned by depositing VN on various substrates. We observed that superconducting transition temperature was enhanced by tensile strain while suppressed by compressive strain. The change of T_c is relatively large, from 6.53 to 8.26 K. We further demonstrate dynamical *in situ* strain tuning by preparing VN films on piezoelectric substrate and adjusting the substrate's lattice constant, for which we are able to achieve control of T_c by a step of 10 mK. DFT calculations found that the $d_{x^2-y^2}$ and d_{xy} orbitals of vanadium atoms are responsible for itinerant electrons. In-plane strain modifies energy levels of the orbitals and their density of states, effectively tuning superconductivity. Our study points to an effective and convenient method to control superconductivity of VN, which can provide a valuable reference for related practical applications. This strain-tuning method can also be further generalized to the other TMN superconductors.

ACKNOWLEDGMENTS

This work was supported by National Key R&D Program of China (Grants No. 2018YFA0305604 and No. 2020YFA0309100), National Natural Science Foundation of China (NSFC) (Grants No. 11874403, No. 11974390, and No. 12174428), Beijing Nova Program of Science and Technology (Grant No. Z191100001119112), Beijing Natural Science Foundation (Grants No. JQ21002 and No. 2202060), and the Guangdong-Hong Kong-Macao Joint Laboratory for Neutron Scattering Science and Technology.

-
- [1] P. M. Tedrow and R. Meservy, *Physica B+C (Amsterdam)* **107**, 527 (1981).
 - [2] H. Rietschel, H. Winter, and W. Reichardt, *Phys. Rev. B* **22**, 4284 (1980).
 - [3] L. E. Toth, C. P. Wang, and G. M. Yen, *Acta Metall.* **14**, 1403 (1966).
 - [4] L. M. Corliss, N. Elliott, and J. M. Hastings, *Phys. Rev.* **117**, 929 (1960).
 - [5] J. D. Browne, P. R. Liddell, R. Street, and T. Mills, *Phys. Status Solidi A* **1**, 715 (1970).
 - [6] Q. Jin, H. Cheng, Z. Wang, Q. Zhang, S. Lin, M. A. Roldan, J. Zhao, J. Wang, S. Chen, M. He *et al.*, *Adv. Mater.* **33**, 2005920 (2021).
 - [7] Q. Jin, Z. Wang, Q. Zhang, J. Zhao, H. Cheng, S. Lin, S. Chen, S. Chen, H. Guo, M. He *et al.*, *Phys. Rev. Materials* **5**, 023604 (2021).
 - [8] R. B. Kaner, J. J. Gilman, and S. H. Tolbert, *Science* **308**, 1268 (2005).
 - [9] B. Navinsek and S. Seal, *JOM* **53**, 51 (2001).
 - [10] X. Marti, I. Fina, C. Frontera, J. Liu, P. Wadley, Q. He, R. J. Paull, J. D. Clarkson, J. Kudrnovský, I. Turek *et al.*, *Nat. Mater.* **13**, 367 (2014).
 - [11] Y. Zhou, W. Guo, and T. Li, *Ceram. Int.* **45**, 21062 (2019).
 - [12] Y. Liu, Q. Wu, L. Liu, P. Manasa, L. Kang, and F. Ran, *J. Mater. Chem. A* **8**, 8218 (2020).
 - [13] K. Robert, D. Stiévenard, D. Deresmes, C. Douard, A. Iadecola, D. Troade, P. Simon, N. Nuns, M. Marinova, M. Huvé *et al.*, *Energy Environ. Sci.* **13**, 949 (2020).
 - [14] M. W. Williams, K. M. Ralls, and M. R. Pickus, *J. Phys. Chem. Solids* **28**, 333 (1967).
 - [15] Y. T. Yemane, M. J. Sowa, J. Zhang, L. Ju, E. W. Deguns, N. C. Strandwitz, F. B. Prinz, and J. Provine, *Supercond. Sci. Technol.* **30**, 095010 (2017).
 - [16] K. M. Bastiaans, D. Chatzopoulos, J.-F. Ge, D. Cho, W. O. Tromp, J. M. van Ruitenbeek, M. H. Fischer, P. J. de Visser, D. J. Thoen, E. F. C. Driessen *et al.*, *Science* **374**, 608 (2021).
 - [17] J. Zasadzinski, R. Vaglio, G. Rubino, K. E. Gray, and M. Russo, *Phys. Rev. B* **32**, 2929 (1985).
 - [18] B. Wang, K. Matsubayashi, Y. Uwatoko, and K. Ohgushi, *J. Phys. Soc. Jpn.* **84**, 104706 (2015).
 - [19] F. I. Ajami and R. K. MacCrone, *J. Phys. Chem. Solids* **36**, 7 (1975).
 - [20] N. F. Berk and J. R. Schrieffer, *Phys. Rev. Lett.* **17**, 433 (1966).
 - [21] B. R. Zhao, L. Chen, H. L. Luo, M. D. Jack, and D. P. Mullin, *Phys. Rev. B* **29**, 6198 (1984).
 - [22] G. N. Gol'tsman, O. Okunev, G. Chulkova, A. Lipatov, A. Semenov, K. Smirnov, B. Voronov, A. Dzardanov, C. Williams, and R. Sobolewski, *Appl. Phys. Lett.* **79**, 705 (2001).
 - [23] A. B. Mei, O. Hellman, N. Wireklint, C. M. Schlepütz, D. G. Sangiovanni, B. Alling, A. Rockett, L. Hultman, I. Petrov, and J. E. Greene, *Phys. Rev. B* **91**, 054101 (2015).

- [24] See Supplemental Material at <http://link.aps.org/supplemental/10.1103/PhysRevB.105.224516> for structure characterization, resistivity and Hall coefficient extracted by simulations, estimate for dirty limit, and analyses of nitrogen content.
- [25] K. Maki, *Phys. Rev.* **148**, 362 (1966).
- [26] A. Gurevich, *Phys. Rev. B* **67**, 184515 (2003).
- [27] E. Helfand and N. R. Werthamer, *Phys. Rev.* **147**, 288 (1966).
- [28] N. R. Werthamer, E. Helfand, and P. C. Hohenberg, *Phys. Rev.* **147**, 295 (1966).
- [29] R. K. Zheng, J. Wang, X. Y. Zhou, Y. Wang, H. L. W. Chan, C. L. Choy, and H. S. Luo, *J. Appl. Phys.* **99**, 123714 (2006).
- [30] R. K. Zheng, H.-U. Habermeier, H. L. W. Chan, C. L. Choy, and H. S. Luo, *Phys. Rev. B* **80**, 104433 (2009).
- [31] R. R. Jia, J. C. Zhang, R. K. Zheng, D. M. Deng, H.-U. Habermeier, H. L. W. Chan, H. S. Luo, and S. X. Cao, *Phys. Rev. B* **82**, 104418 (2010).